Topographic mapping of the moon via a radar system

A. Coradini (*), R. Cramarossa (**), P. Lombardo (**), G. Picardi (**), R. Seu (**)

(*) IAS Rep. Planetologia, V.le dell'Universita' 11, 00185 Rome, ITALY
(**) INFO-COM Dpt, University of Rome "La Sapienza"
Via Eudossiana 18, 00184 Rome, ITALY

ABSTRACT

The paper deals with the design of the radar mapping system for the MORO mission proposal. The system is able to operate both in an altimetric mode and in an interferometric SAR mode to provide respectively low and high resolution topographic mapping of the moon surface. As a matter of fact either a topographic map of the lunar surface with a spatial resolution better than 1 km and a higher accurate (better than .5 m) measure of the surface height and a topographic map with better spatial resolution (about 20 m, comparable with optical systems) and a lower vertical resolution (in the order of a few meters) have been envisaged as very important goals of the mission. Actually the spinning platform selected for the mission makes the system design challenging. Nevertheless, after a careful analysis, it is shown that the radar can still meet the 3-D mapping requirements. Moreover the possibility of the simultaneous operativity of SAR and altimeter is analysed. The main parameters to assure this joint mapping are set and the system performance in this condition assessed.

1. INTRODUCTION

In response to a specific call issued by ESA, a group of European researchers submitted a proposal for a Moon ORbiting Observatory (the so called MORO mission) which passed a first selection [1]. Among the on board instruments there is a radar system, named LUMI (LUnar Microwave Instrument), to be used for the production of topographic lunar maps. To obtain the desired 3-D imaging of the moon, LUMI has been provided with two mapping modes:

- low resolution mode (LRM)
- high resolution mode (HRM)

In the LRM the mapping is obtained by means of a radar altimeter, which operates in pulse limited configuration. While a low horizontal resolution is obtained in this mode, the estimate of the mean height inside the resolution cell is performed with very high accuracy. The HRM makes use of a SAR (synthetic aperture radar) to achieve the high horizontal resolution. The height information is provided by the interferometric processing of multiple SAR images obtained from different orbits.

The radar altimeter, other than a mapping device, is an essential support for most of the other instruments on board because it provides an accurate height reference for them. Since the selected spacecraft is a spinned satellite the interferometric SAR (INSAR) mode becomes the main high resolution mapping instrument. In fact, unlike the stereo cameras, that seem to be highly affected from the rotation of the platform, the performance of the INSAR suffers only small degradation, as it will be shown in the following.

Nevertheless the use of a spinned satellite, without an antenna stabilisation, results in a challenging design for the dual-mode radar sensor. As a matter of fact only for a small fraction of the platform rotation time the antenna beam is directed towards the moon surface. The extraction of all the information necessary for the mapping from the short time available is addressed in the paper. In particular, after a quick review of the main characteristics of the mission is given in Section 2, the design of the two mapping modes is addressed. System design and analysis of the system performance in the LRM and HRM, with specific attention to the problems caused by the spinning platform, are presented in Section 3 and 4 respectively. The possibility to obtain the simultaneous operativity of the two mapping modes, using a switching dual-beam antenna is presented in Section 5. Particular attention is devoted to the choice of the pulse repetition frequency (PRF), whose careful selection can allow to interlace transmission and reception of the pulses of radar altimeter and SAR making an optimum use of the available operative time.

2. THE MORO MISSION

MORO is a lunar polar orbiter able to perform remote sensing observations of the lunar surface and measurements of the global topography and gravimetry of the moon. It will allow to obtain at the same time high resolution imaging together with high quality data on lunar mineralogy and topography. The MORO spacecraft is designed to carry five experiments: a stereo camera, an UV-visible and IR mapping spectrometer, a γ-ray spectrometer, LUMI and to release a subsatellite for gravimetric experiments [1].

In particular the remote sensing instruments are designed to study the lunar surface in an entirely new way, allowing to obtain 3D high resolution imaging of the moon coupled with topographic data. Modelling of gravity field, geodesy, the estimate of the thickness of geologic units, spaceflight engineering and operations and other important scientific and technical tasks depend on the knowledge of lunar topography. Remote sensing techniques both spaceborne and recently ground based were used in the past to acquire a large scale description of the moon surface, in order to characterise the moon as a global entity. US lunar orbiters (Apollo 11 to 17 missions) provided indispensable photographic coverage of most of the moon from their near polar orbits. Unfortunately the heights of basin rims and other rings and the elevations of contained maria are particularly significant but yet the topography of no basin has been completely determined. Refinements of the topography of the near side still depend on telescopic selenodesy. The topography of the parts of the far side and the polar regions, that were not overflown, is almost completely unknown and the need for these data is obvious. The LRM will provide large scale 3-D imaging of the global moon surface. Moreover the altimeter can provide an accurate measure of the dielectric properties of the imaged surface together with its geometrical roughness. To obtain a higher resolution topographic mapping the use of photogrammetric instruments, coupled to the height reference provided by the LRM, was proposed. Indeed, since the height resolution of the stereo cameras seems to be severely affected from the spinning of the platform, the HRM could represent the desired improvement of the mission. Moreover, optical systems can be used only for the illuminated parts of the orbit groundtracks and the HRM becomes essential whenever bad illumination conditions occur. In particular among the regions which are always in this condition there is one of the poles, which seems to be rich of information and, as mentioned above, has not yet been mapped.

A cluster-based spacecraft has been selected for the mission [1]. Its stabilisation is achieved in the operational orbit by spinning the satellite at 5 rpm (angular speed = 30 deg/sec.). The lateral side of the cylinder points towards the surface of the moon, while the spin axis is kept perpendicular to the orbit plane. The instruments have their open field of view on the cylinder lateral surface, therefore they have a direct view to the moon surface once per spin revolution, i.e. every 12 seconds. The proposed orbit is a circular near polar orbit at an altitude of H = 100 Km, which is flown from the spacecraft at an average speed of v = 1632 m/s.

3. SPINNED ALTIMETER (LRM)

The main requirements for the LRM are:

• ground resolution	$\leq$ 1000 m
• height measurement accuracy	$\leq$ 0.5 m
• height resolution	$\leq$ 1 m
• noise equivalent σ^0 (single pulse)	$\leq$ -10 dB
• surface roughness accuracy	$\leq$ 15%

In this mode the antenna is pointing at nadir (or better perpendicularly to the spin axis) and, as mentioned in the introduction, the radar system is working as a pulse limited altimeter. As a matter of fact a very large antenna (in the order of two meters) would be necessary to obtain the required horizontal resolution using a conventional beam-limited altimeter. On the contrary it is strightforward to relax the constraints on the antenna size by using the radar transmitted waveform to synthesise an equivalent beamwidth much smaller than the antenna footprint. With reference to figure 1 the first echo from the ground contains the backscattering contribution only from a small disk of diameter

$$2R_p = 2\sqrt{(H+\delta)^2 - H^2} \approx 2\sqrt{2\delta H} \qquad (1)$$

where δ is the compressed radar pulse. Unlike the first, successive echoes, corresponding to the same transmitted pulse, contain the contribution from circular concentric rings, whose diameter is progressively increasing. If δ is short enough, so that R_p is much smaller than the antenna footprint dimension, taking only the first echo it is possible to select an area corresponding to a narrower equivalent beam $\vartheta_{eq} \cong R_p / H$. In the specific situation, using the same bandwidth for the transmitted chirp waveform of ERS1

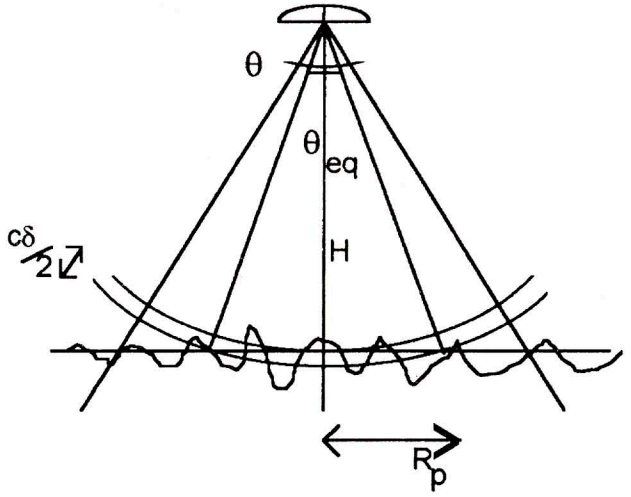

Figure 1 - Pulse limited altimeter geometry.

(B = 330 MHz, [2]), it results a compressed pulse length $\delta = c/2B = 0.45\ m$ (c being the speed of the light), which defines the height resolution. The horizontal resolution is therefore R_p = 600 m, corresponding to a $\vartheta_{eq} = 6mrad$ (0.34 deg). While the vertical resolution is given by δ, the accuracy can be much higher, due to the tracking of the surface in successive pulses. The above figures show clearly a performance well inside the mission requirements for the LRM. The effect of platform spinning does not affect the resolution, but makes impossible a complete pulse limited mapping. As a matter of fact, with reference to figure 2, only when the real beam contains the whole narrow equivalent pulse limited beam pointing at nadir, the first echo from the surface is correctly received and the system is working as illustrated above. Only a lower resolution mapping is possible when this condition is no longer verified, since the echoes are backscattered from thin strips – portions of the mentioned rings – which cannot give a good resolution in the cross track direction. To assure a complete coverage, at least at the lowest resolution, the antenna footprint in the along-track direction is selected to be equal to the translational motion of the spacecraft during a half revolution time and two antennas are used, allocated with an angular displacement of 180 degrees in the satellite

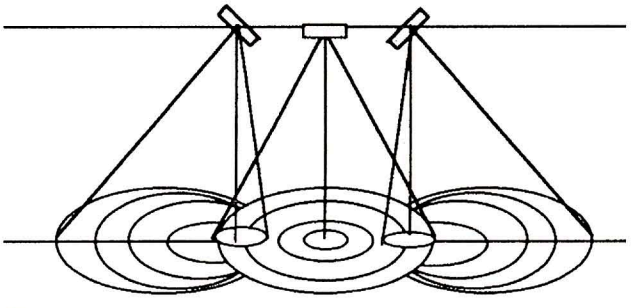

Figure 2 - Altimetry from spinned platform.

cylindrical surface. Therefore the revisitation time is T = 6 s and the antenna beamwidth in the along-track direction is selected to be equal to $\vartheta = vT/h = 98mrad$ (5.6 deg). Assuming a wavelength $\lambda = 2.17\ cm$ (as in the Cassini mission [3]), the corresponding antenna dimension is set to D = 22 cm. This assures a complete coverage of the radar LRM even if only partially done with the maximum resolution and accuracy. The dwell time on the pulse limited footprint can be evaluated as the time needed to the spacecraft to rotate from the two extreme positions $\pm\xi_m$, symmetric with respect to nadir, where

$$\xi_m = \frac{\vartheta - \vartheta_{eq}}{2} = 46mrad \quad (2.63 \text{ deg}) \tag{2}$$

The dwell time is therefore $T_m = 2\xi_m/\omega = 0.17\ s$ and, since the spacecraft moves only 277 m during this time, only one resolution cell is mapped every half rotation, which corresponds to mapping, in pulse-limited mode, about a 6% of the lunar surface each orbit. To achieve a low power consumption the radar can be maintained on power only during this time resulting in an equivalent duty cycle of $T_m/T = 2.9\%$. The PRF of the radar altimeter has been selected as the maximum PRF, such that two contiguous echoes can still be considered uncorrelated [4] (see also App. 1 and [5])

$$PRF \leq 5.1 \frac{v}{\lambda} \sqrt{\frac{\sigma_s}{H}} \tag{3}$$

Assuming that the portion of lunar surface inside the antenna footprint can be modelled as a gaussian random surface with a minimum standard deviation $6_s \approx 1.5\ m$ and provided that for the selected orbit of 100 km height (H) the spacecraft speed must be about v = 1632 m/s [6], the PRF is set at 1500 Hz. The number of radar pulses which can be integrated by the system to obtain the maximum accuracy is therefore $N_I = PRF \cdot T_m$. The average height of the lunar surface in the resolution cell can be obtained via a maximum likelihood estimate based on the processing of the available N_I pulses. In order to obtain the performance of this processor the samples of the return echoes are modelled as exponentially distributed random variables with a mean value expressed as a function of the delay time τ referred to the mean surface echo delay [7], [8]

$$P(\tau) = k_r \sigma_0 e^{-\frac{4}{\vartheta_a} \sin^2 \xi} \left[1 + erf\left(\frac{\tau}{\sigma_c \sqrt{2}} \right) \right] \cdot e^{-\frac{4cx}{\vartheta_a H} \cos(2\xi)} \cdot I_0 \left[\frac{4}{\gamma} \sqrt{\frac{cx}{H}} \sin(2\xi) \right] \tag{4}$$

where

- $x = \begin{cases} 0 & \tau \le 0 \\ \tau & \tau > 0 \end{cases}$
- $\sigma_c^2 = (0.425 / B)^2 + (2\sigma_s / c)^2$
- ϑ_a is related to the antenna beamwidth by defining the antenna gain as $G(\gamma) = \exp\left[-2.8\frac{\gamma^2}{\theta_a^2}\right]$
- k_r is a power parameter given by the radar equation
- $I_0[..]$ is the modified Bessel function first kind, zeroth order.

4. SAR INTERFEROMETRY

Before facing the problems related to the interferometric processing, we want to discuss the design of the main parameters for the SAR, devoting particular attention to the effect of the platform spinning. The main requirements for the radar HRM are

• ground resolution	< 20 m
• height measurement accuracy	< 5 m
• height resolution	< 50 m
• Noise equivalent 6°	< -10 dB
• radiometric resolution	< 1 dB

The required horizontal resolution is easily obtained in the cross-track direction (r_x) via pulse compression. Since the bandwidth of the transmitted pulse, selected for the altimeter, is much higher than the one necessary to obtain the desired resolution, it is possible to split it to obtain a number of independent images with the required resolution at slightly different frequencies. Averaging the different images yields a multilook image which easily achieves the required radiometric resolution. Even if the final selection of the off-nadir angle α_0 (angle between the perpendicular to the radar and the centre of the antenna footprint) will be discussed later in the paper after the analysis of the PRF diagram, let us now assume the likely value $\alpha_0 = 30$ degrees. In this case to obtain the required resolution a synthetic aperture L_s is necessary given by

$$L_s = \frac{\lambda H}{2 r_y \cos\alpha} = 62.6\,m \qquad (5)$$

where r_y (usually equal to r_x) is the along-track ground resolution. Given the orbit parameters, while the spacecraft moves of L_s it rotates of only 0.36 degrees, which is well contained within the 5.6 degrees of the beamwidth. It is therefore evident that the required resolution can easily be achieved also in the along-track direction despite the spacecraft is spinning. The only condition necessary to assure the complete coverage is an overlapping between the antenna footprints after a half rotation of at least L_s. Since in a half rotation the spacecraft moves of vT = 9.8 Km and the along-track dimension of the footprint is $\frac{\lambda H}{D\cos\alpha_0} = 11.4\ Km$ the overlapping is more than the required one, at least for the central part of the swath in the cross-track direction (Figure 3). This suggests that even more than one look images can be obtained. At the extremities of the cross range swath the overlapping condition is not verified any more, in fact, due to the satellite spinning the centre swath, as well as its extremities depend on the rotation angle. Assume as a reference the condition in which the antenna pointing is normal to the spacecraft track, the angle σ can be defined which identifies the rotation of the satellite around its axis. Due to the spin the beam pointing moves from the direction orthogonal to the track as σ moves from its reference and the centre swath moves in the along track direction of

$$\gamma(\sigma) = H \cdot tg\sigma \qquad (6)$$

with respect to the spacecraft position, passing from forward to backward. The off-nadir angle changes as $\alpha(\sigma) = \arccos(\cos\alpha_0 \cdot \cos\sigma)$ causing the extrema of the footprint in the cross-track direction to be a function of σ

$$x_{\min} = \frac{tg\alpha_0}{\sqrt{tg^2\alpha_0 + \sin^2\sigma}} \cdot H \cdot tg\left[\alpha(\sigma) - \frac{\gamma}{2}\right] \qquad (7)$$

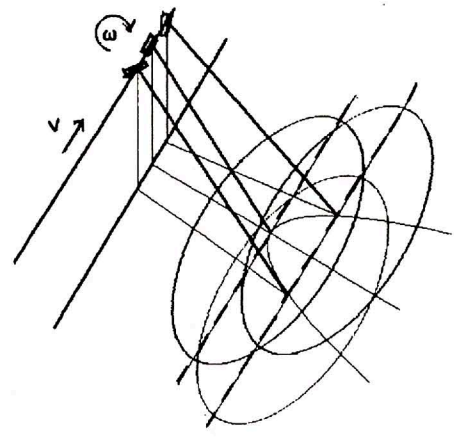

Figure 3 - SAR from spinned platform.

$$x_{max} = \frac{tg\alpha_0}{\sqrt{tg^2\alpha_0 + sin^2\sigma}} \cdot H \cdot tg\left[\alpha(\sigma) + \frac{\gamma}{2}\right] \quad (8)$$

where γ is the antenna beamwidth in the cross-track direction. The behaviour of eq (7) and (8) is shown in figure 4, where the antenna cross-track dimension has been set to L = 0.5 m resulting in $\gamma = \lambda / L = 43 mrad$ (2.5 deg). It is easy to realize from it the presence of a large strip of the scene continuously imaged by the SAR. The spinned platform causes only some loss at the extrema of the swath in the cross range direction. An additional slight drawback of the spinned platform is the presence of a much stronger effect of amplitude modulation of the return echoes from the rotating antenna, which might cause slight resolution losses. The main parameter which remains to be set is the SAR PRF. Two bounds control its choice: the Nyquist sampling of the clutter spectrum seen from the antenna sets the lower bound

$$PRF \geq \frac{2v}{D} \approx 13\ KHz \quad (9)$$

where D has been set equal to 0.25 m.

The upper bound is given by the need to keep unambiguous all the cross-track swath dimension

$$PRF \leq \frac{c \cdot L \cdot \cos\alpha_0}{2\lambda \cdot H \cdot tg\,\alpha_0} \approx 24\ KHz \quad (10)$$

A PRF of 15 KHz seems to be a good choice for the system allowing to maintain some margins without overloading the data rate. This value is only indicative of course and must be checked by taking into account the order of ambiguity of the return echoes and the Altitude Line Echo (ALE or nadir returns) problems [9], [10]

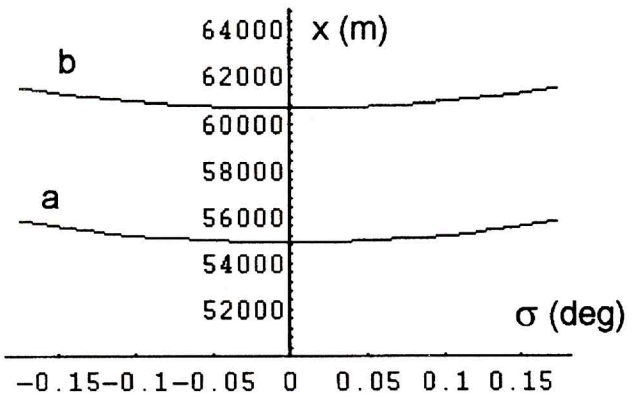

Figure 4 - Motion of the extrema of the cross-range swath: $a = x_{min}$, $b = x_{max}$

The height resolution, as mentioned in Section 1, is obtained via the coherent processing of multiple SAR images of the same scene obtained in different orbits horizontally displaced by a length B_s, called baseline. The height information is basically derived exploiting the relationship between the pixel height q_i (measured with respect to a reference plane) and the phase difference $\Delta\Psi_i$ of the single pixel in the two complex SAR images (see figure 5)

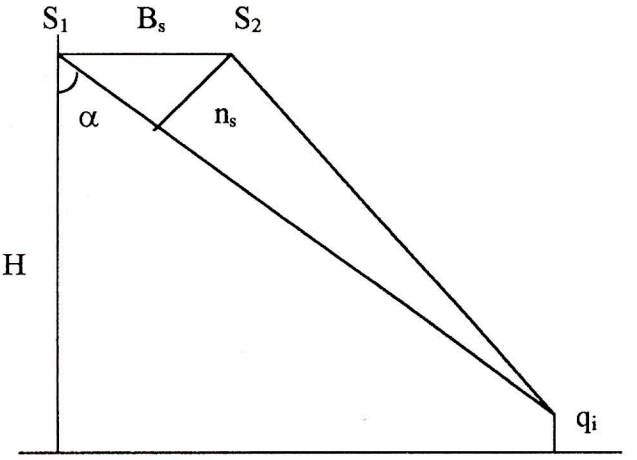

Figure 5 - Geometry for interferometric SAR.

$$q_i \approx \frac{\lambda \cdot H \cdot tg\,\alpha_0}{4\pi \cdot n_s} \cdot \Delta\Psi_i \quad (11)$$

where n_s is the component of the horizontal baseline B_s in the direction normal to the slant range axis. The height resolution Δ_q is approximately obtained from eq (11) as the value of the height relative to a phase change of 2π [11]

$$\Delta q \approx \frac{\lambda H \cdot tg\,\alpha_0}{2\,n_s} = \frac{\lambda H \cdot tg\,\alpha_0}{2B_s \cos\alpha_0} \quad (12)$$

Therefore to obtain a height resolution equal to or better than the one required for the HRM the baseline must be $B_s > 14.5$ m which does not represent a limitation for the present situation. On the contrary a higher bound on the choice of the baseline is given from the necessity to compare the phases of two scenes still sufficiently correlated to each other. To derive this second bound lets observe that to the first order the eq (11) represents also the relationship between the errors on the estimate of the height σ_q and of the phase $\sigma_{\Delta\Psi}$, once q_i and $\Delta\Psi_i$ have been replaced with σ_q and $\sigma_{\Delta\Psi}$ respectively. The error on the phase estimate in the presence of thermal noise and by considering a processing based on N_L looks can be shown to be [12]

$$\sigma_{\Delta\Psi} = \frac{1}{\sqrt{2N_L}} \cdot \frac{\sqrt{\left(1 + SNR^{-1}\right) - \rho^2}}{\rho} \tag{13}$$

where SNR is the signal to noise ratio and ρ is the modulus of the complex correlation coefficient between the two images $F_1(x_0, y_0)$ and $F_2(x_0, y_0)$ conventionally defined as

$$\rho = \frac{\left|\left\langle F_1(x_0, y_0) \cdot F_2^*(x_0, y_0)\right\rangle\right|}{\left\langle \left|F_1(x_0, y_0)\right|^2 \right\rangle^{1/2} \left\langle \left|F_2(x_0, y_0)\right|^2 \right\rangle^{1/2}} \tag{14}$$

Assuming that the SAR point target response is given by $W(x, y) = sinc(\pi x/r_x)sinc(\pi y/r_y)$ and in the hypothesis of a white gaussian uncorrelated scene, it yields [12]

$$\rho = (1 - \delta) \cdot sinc(\pi\vartheta_x) \cdot sinc[\pi\vartheta_y (1 - \delta)] \tag{15}$$

where ϑ_x, ϑ_y are the misregistration errors in cross and along-track directions expressed in fractions of resolution cell and the so called decorrelation parameter

$$\delta = 2 \cdot \frac{r_y n_s \cos^2\alpha_0}{\lambda H} \tag{16}$$

takes into account for the decorrelation due to the different observation angle of the single pixel in the two orbits. To set the bounds for the baseline the normalised error $e_n = \sqrt{N_L}\sigma_q/r_y$ [12] is shown in figure 6 for different SNRs and misregistrations. As it is evident from the figure once a maximum value has been fixed for the normalised error e_n, the range of variation of δ is constrained. Since there is a linear relation between δ and the baseline B_s, also the bounds for B_s are obtained. To achieve the required height accuracy of 5 m with a horizontal resolution of 20 m and in the hypothesis of $N_L = 4$ looks the threshold on e_n is set to 0.5, which is obtained with a decorrelation δ between 0.25 and 0.75, having assumed a SNR of 10 dB and misregistration of 0.3 pixels. The admissible values of the baseline to match the requirements are therefore approximately between 21 m and 63 m. The requirement for coarser spatial resolutions or height accuracy would obviously relax the constraints on the orbit allowing to longer baselines. A drawback caused from the spinned platform is that in successive orbits it is not likely for the radar to image the single point in the scene from the same horizontal angular direction, due to the small equivalent duty cycle. If this mismatch is small we may refer to the discussion reported in [13] since an angular mismatch corresponds to a doppler frequency mismatch and conclude that the effect is a further decorrelation term to be taken into account. The term is expected to act in similar way of the former, representing the decorrelation in the horizontal plane instead that in the vertical one. Its effect is expected anyway to be small at least for sensible displacements of the platform[1].

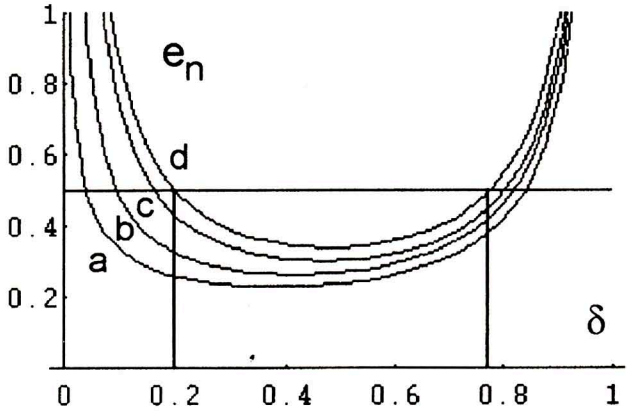

Figure 6 - Normalised height error e_n Vs decorrelation δ for: a) SNR = ∞, ϑ_x, ϑ_y = 0; b) SNR = 10 dB, ϑ_x, ϑ_y = 0; c) SNR = ∞, ϑ_x, ϑ_y = 0.3; d) SNR = 10 dB, ϑ_x, ϑ_y = 0.3.

It can be concluded therefore that the interferometric SAR above can meet the requirements for the HRM, nevertheless the platform is spinned.

5. INTERLACING ALTIMETER AND SAR-IN

After having set the main design parameters for the radar system in the two modes LRM and HRM it remains to be shown how the two modes can operate simultaneously. To obtain this result an antenna able to commute its pointing from the nadir to the 30 degrees off-nadir angle, in times in the order of a μs has to be selected. This allows to commute between LRM and HRM on a pulse to pulse basis. Two different solutions have been identified to obtain this result. The first is to use a phased array with approximately 23 x 46 elements driven by ferrite phase shifters. The great flexibility of this solution has drawbacks in terms of weight and power consumption. The other possible solution is to use two horn antennas 30 degrees apart connected to the same transmit-receiver module by means of a ferrite power switch. The latter solution, nevertheless is less flexible and provides a smaller decoupling between the two modes, shows some advantages in cost, power

1. In any case it is worthwhile to mention that we shall have in general a number of images of the same site greater than 2 and we may select in principle the best ones by the analysis of the interference fringes.

consumption and reliability and seems to be the favourable solution to the problem.

The difference of about an order of magnitude between the PRFs selected for the two modes suggests to transmit and receive a set of SAR pulses for each altimeter pulse. The problem in handling at the same time SAR and altimeter pulses avoiding superposition made more serious from the fact that SAR PRF has been chosen so that the system is receiving pulses corresponding to the transmission done a number of pulse repetition times before (the radar is ambiguous in range). We will therefore identify the admissible regions of PRF for either SAR and altimeter and chose the dual – mode system PRF in their intersection. This will assure the possibility to operate at the same time the two modes without collisions, except the unavoidable loss of two SAR pulses when the altimeter is transmitting or receiving. Let us now evaluate the minimum and maximum delay respectively for altimeter and SAR as follows

$$T_{min}^{ALT} = \frac{2H}{c} \tag{17}$$

$$T_{max}^{ALT} = \frac{2H}{c} \cdot \frac{1}{\cos(\vartheta/2)} \tag{18}$$

and

$$T_{min}^{SAR} = \frac{2H}{c} \cdot \frac{1}{\cos(\alpha_0 - \gamma/2)} \tag{19}$$

$$T_{max}^{SAR} = \frac{2H}{c} \cdot \frac{1}{\cos(\alpha_0 - \gamma/2)} \tag{20}$$

The requirements to avoid the loss of some part of the received echo for the altimeter are

$$\begin{cases} T_{min}^{ALT} \geq \dfrac{j}{PRF} + \tau \\ T_{max}^{ALT} \leq \dfrac{j+1}{PRF} - \tau \end{cases} \Rightarrow \begin{cases} PRF \geq \dfrac{j}{T_{min}^{ALT} - \tau} \\ PRF \leq \dfrac{j+1}{T_{max}^{ALT} + \tau} \end{cases} \tag{21}$$

where τ is the uncompressed pulse length and the integer j represents the order of ambiguity for the altimeter. The analogous for the SAR are

$$\begin{cases} T_{min}^{SAR} \geq \dfrac{i}{PRF} + \tau \\ T_{max}^{SAR} \leq \dfrac{i+1}{PRF} - \tau \end{cases} \Rightarrow \begin{cases} PRF \geq \dfrac{i}{T_{min}^{SAR} - \tau} \\ PRF \leq \dfrac{i+1}{T_{max}^{SAR} + \tau} \end{cases} \tag{22}$$

where i represents the order of ambiguity for the SAR. The regions above are shown in figure 7 as a function of the off-nadir angle α_0 within the range of admissible PRF's for the SAR, provided by the eq (9) and (10). The regions jointly admissible for the two modes are highlighted (by means of a simple shadowing), representing possible PRF choices. In particular a PRF between 14 and 14.5 KHz is chosen for the system, decreasing the off-nadir angle at about 25 deg. The desire to avoid the presence of the altitude line echo (ALE) would require the further constraints to be respected

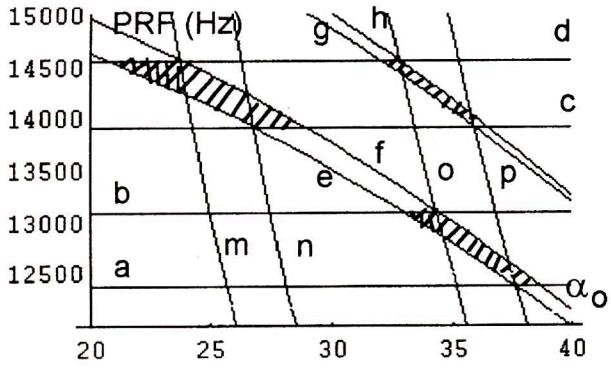

Figure 7 - System PRF selection diagram. Lower and upper bound on the PRF are shown respectively for altimeter (j = 8) a)-b) and (j = 9) c)-d), SAR (i = 10) e)-f) and (i = 11) g)-h). The highlighted region is the zone of joint admissibility. The ALE constraints are m) upper bound (l = 1); n)-o) lower and upper bound (l = 2); p) lower bound (l = 3). The triangular highlighted regions are the admissible ALE free zones.

$$\begin{cases} T_{min}^{SAR} \geq \dfrac{l}{PRF} + \dfrac{2H}{c} \\ T_{max}^{SAR} \leq \dfrac{l+1}{PRF} + \dfrac{2H}{c} \end{cases} \Rightarrow \begin{cases} PRF \geq \dfrac{l}{T_{min}^{SAR} - \dfrac{2H}{c}} \\ PRF \leq \dfrac{l+1}{T_{max}^{SAR} - \dfrac{2H}{c}} \end{cases} \tag{23}$$

being *l* the order of ambiguity of the ALE. In order to satisfy also eq (23) the admissible regions must be reduced to the small triangular regions that can be identified in figure 7 being highlighted with a double shadowing. Since the choice would become too sensitive to the off nadir angle the ALE will be more simply avoided maintaining a null of the antenna radiation pattern at nadir.

The last problem to be faced is the evaluation of the SAR point target response when 2 out of 10 echoes are missing as already mentioned above. Since the orders of ambiguity of the altimeter and SAR are respectively 9 and 10 (j = 9, i = 10 in the selected region of figure 7), the two missing echoes are adjacent and the effect can be taken into

account, pretending that the SAR echo sequence is modulated from a square-wave with a duty cycle of 80%. Assuming that all the echoes are received, the signal sequence received from the SAR observing a point target during the synthetic aperture time can be represented as the chirp signal

$$x(t) = e^{j\pi \frac{B_a}{T_0} t^2} \qquad -\frac{T_0}{2} \le t \le \frac{T_0}{2} \tag{24}$$

where $T_0 = L_s / v$ and $B_a = v / r_x$. The received signal when the 2 pulses are missed can be written as $s(t) = x(t) \cdot y(t)$ where the modulating square wave y(t) is expressed by means of its decomposition in terms of spectral components, as

$$y(t) = \frac{8}{10} \sum_{n=-\infty}^{\infty} \frac{\sin(\pi n\, 8/10)}{\pi n\, 8/10} e^{-j2\pi \frac{n}{10} PRF \cdot t} \tag{25}$$

After the azimuth compression operation, which consists basically in passing s(t) through a filter matched to the waveform eq (24), the azimuth point target response is given by [14]

$$g(t) = \sqrt{B_a \tau}\, \frac{8}{10} \left| \sum_{n=-\infty}^{\infty} \frac{\sin(\pi n\, 8/10)}{\pi n\, 8/10} \cdot e^{-j\pi \frac{n}{10} PRF \cdot t} \right.$$
$$\left. \cdot \frac{\sin\left[\pi B_a (t - n\, PRF/10 \cdot T_0 / B_a) \cdot (1 - |t| / T_0)\right]}{\pi B_a (t - n\, PRF/10 \cdot T_0 / B_a)} \right| \tag{26}$$
$$-T_0 \le t \le T_0$$

It is instructive to observe g(t): the whole response is obtained as the sum of a set of terms given by the autocorrelation function for the complete echo sequence (second term in (26)) translated of $t_n = nPRF/10 \cdot T_0/B_a$ and weighted by the Fourier series component of the square wave at frequency n/10. The term for n = 0 is the desired response, which corresponds to the zero frequency component of the modulating square wave. It would be the only component present in the (constant) modulating waveform in absence of missing sample and with respect to that condition it appears reduced by 8/10 (~1dB). The other terms in the sum are the paired echoes corresponding to the successive frequency components of the square wave and in fact the shift t_n is given by a number of resolution cells $^/B_a$ equal to the ratio between the total integration time T_0 and period of y(t), i.e. the fundamental component of the modulating waveform. The paired echoes are therefore centred at t = t_n and since they are enough displaced from each other their amplitude is given approximately by

$$\sqrt{B_a T} \cdot \frac{8}{10} \cdot \frac{\sin(\pi n\, 8/10)}{\pi n\, 8/10} \tag{27}$$

resulting in a maximum sidelobe about 6.38 dB below the peak. This is the real limitation caused by the joint operativity of the two modes. To avoid this drawback two actions can be done: (i) use a lower PRF for the altimeter, resulting in a lower accuracy for the height estimation in the LRM; (ii) control the sidelobe level during the pulse compression using a weighting network which subtracts from g(t) shifted and scaled versions of itself to counteract the sidelobes. As demonstrated in [15] by means of this latter technique an improvement in the peak to sidelobe ratio up to 10-11 dB can be easily obtained. It is moreover interesting to observe that the spin has no influence on the SAR resolution

CONCLUSIONS

The design of a dual mode radar system for the 3-D mapping of the lunar surface in the context of the MORO mission has been presented. The radar altimeter and the interferometric SAR have been shown to meet the requirements for the mapping in LRM and HRM respectively. In particular the effect of the platform spinning on the system performance in the two modes and on the achievable mapping coverage have been studied. Moreover the possibility to operate simultaneously the two modes has been asserted, even if with some performance degradation, and the main parameters have been chosen to allow this joint operation.

ACKNOWLEDGEMENT

The authors would like to thank the Oerlikon-Contraves S.p.a. for useful discussions on the radar antenna configuration

APPENDIX 1

The decorrelation distance in a radar altimeter can be evaluated by considering the geometry of figure A.1 (see also [5]) where the radar is flying at an altitude H over a waveless sea. The contribution to the received echo due to a scattering element on the surface (the point P for instance)

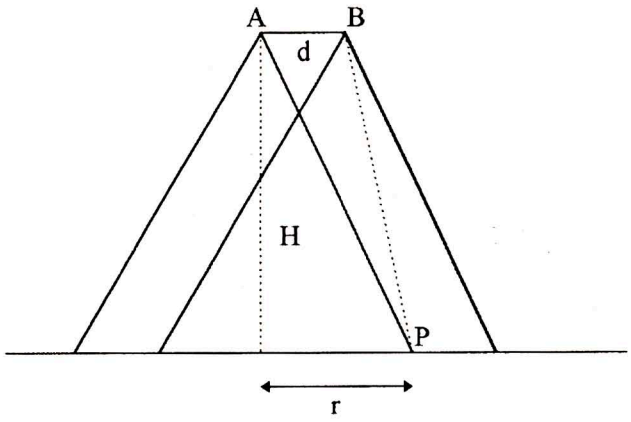

Figure A.1 - Geometry for the evaluation of the decorrelation distance d.

is different in the case of A and B because of a phase term $\Delta\phi$ which is proportional to the distance d. As a matter of fact from the geometry depicted in figure A.1 and by means of very simple arithmetic manipulations, we can write

$$\Delta\phi = \frac{4\pi}{\lambda} \cdot \left(\overline{PA} - \overline{PB}\right) \approx \frac{4\pi}{\lambda} \cdot \frac{rd}{H} \qquad \text{(A.1)}$$

and by letting $\Delta\phi$ equal to a fraction k of 2π and remembering that for a pulse limited altimeter $r \approx \sqrt{2\delta H}$ where δ is the radar range resolution, we obtain

$$d \approx \frac{1}{k} \cdot \frac{1}{2\sqrt{2}} \cdot \frac{\lambda\sqrt{H}}{\sqrt{\delta}} \qquad \text{(A.2)}$$

that is in terms of decorrelation PRF (Pulse Repetition Frequency)

$$PRF \approx k \cdot 2\sqrt{2} \cdot \frac{v}{\lambda} \cdot \frac{\sqrt{\delta}}{\sqrt{H}} \qquad \text{(A.3)}$$

(v being the spacecraft velocity)

which is fully consistent with the results given in [5]. Moreover, as discussed just in [5] the effect of a rough sea surface can be modeled as a worse range resolution δ of the radar and in particular it can be demonstrated that in eq. (A.3) δ can be substituted with the standard deviation of the rise time of the leading edge of the mean return pulse, that is $\sigma_r = \sqrt{\delta^2 + \sigma_h^2}$ if σ_h is the standard deviation of the wave height. By considering that in general δ is smaller (or of the same order) than σ_h and by giving to the constant k a suitable value we obtain the eq.(3) which is in turn fully in agreement with [5]. It is worth noting that, with the necessary differences in the operating geometry, the same approach leads to the important definition of the baseline decorrelation [12] in interferometric processing.

REFERENCES

[1] ESA, M3 Selection process. Presentation of Assessment Study results, Document number SCI(94)9, May 1994.

[2] Losquadro G., Picardi G., Pozzolini G. & Somma R., "The radar altimeter for ERS-1 satellite", International Radar Symposium India, Bangalore, IRSI 83, pp 393-398.

[3] Announcement of Opportunity OSSA-2-89, JPL PD699-11, Vol.VIII, Titan Radar Mapper Description, Oct. 1989.

[4] "Feasibility study of an advanced terrain tracking altimeter", Final Report ESTEC Contract Number 7199/87/NL-JS, March 1989.

[5] Walsh E. J., "Pulse to pulse correlation in satellite radar altimeters", Radio Science, Vol. 17, n° 4, July-August 1982, pp. 786-800.

[6] Racca G. D. ed., "MORO Assessment Study Technical Report", ESA/ESTEC PF/TR/0934, Noordwijk, The Netherlands, June 1994.

[7] G.S. Brown, "The average impulse response of a rough surface and its application", IEEE Trans. on Antennas and Propagation, Vol. 25, n° 1, January 1977, pp. 67-74.

[8] Montefredini E., Morelli F., Picardi G. & Seu R., "A non-coherent surface backscattering model for radar observation of planetary bodies and its application to Cassini radar altimeter", Accepted for publication on Planetary and Space Science.

[9] Picardi G., "Radar Signal Processing", F. Angeli Editore, 1988 (in italian).

[10] Raney R. K., "Conceptual Design of satellite SAR", Proceedings of IGARSS '84 Symposium, Strasbourg 27-30 August 1984.

[11] Prati C. & Rocca F., "Limits to the resolution of elevation maps from stereo SAR images", Int. Journal of Remote Sensing, Vol 11, n° 12, 1990, pp. 2215-2235.

[12] Rodriguez E. & Martin J.M., "Theory and design of interferometric synthetic aperture radars", IEE Proc. Pt. F, Vol. 139, n° 2, April 1992, pp 147-159.

[13] Zebker H.A. & Villasenor J., "Decorrelation in interferometric radar echoes", IEEE Trans. on Geoscience and Remote Sensing, Vol. 30, n° 5, September 1992, pp. 950-959.

[14] Pezzano R., Picardi G., Seu R. & Zompanti N., "Moro: spinned altimetry and interlaced altimeter SAR operations", INFO-COM Dpt Technical Report n° 004-5-94, July 1994.

[15] Bucciarelli T., Boni C. & Richard M., "Optimization of array antennas" and "Synthesis of very large bandwidth waveforms for high resolution radars", INFO-COM Dpt Technical Report n° 005-7-90, Feb. 1990.